Supporting Information

Phonon Dispersion Relation of Bulk Boron-Doped Graphitic Carbon

Devin McGlamery†, Alexander A. Baker‡, Yi-Sheng Liu‖, Martín A. Mosquera†, and Nicholas P. Stadie†*

†Department of Chemistry & Biochemistry, Montana State University, Bozeman, Montana, 59717, United States

‡Materials Science Division, Lawrence Livermore National Laboratory, Livermore, California, 94550, United States

‖Advanced Light Source, Lawrence Berkeley National Laboratory, Berkeley, California, 94720, United States

*Corresponding author: nstadie@montana.edu

Contents:

1. X-Ray Diffraction (XRD)

Analysis of the as-measured XRD patterns (RD) was accomplished by direct subtraction of the background (BGD) based on an identical experiment performed without any sample. The resulting pattern (BGSD) was fitted to the combination of a linear background (BG), a single Lorentzian for the (002) reflection (referred to as L_1), and two Lorentzians for the (10) region (referred to as L_2 and L_3) comprised of the (100) and (101) reflections of crystalline graphite. A representative example is shown in **Figure S1**.

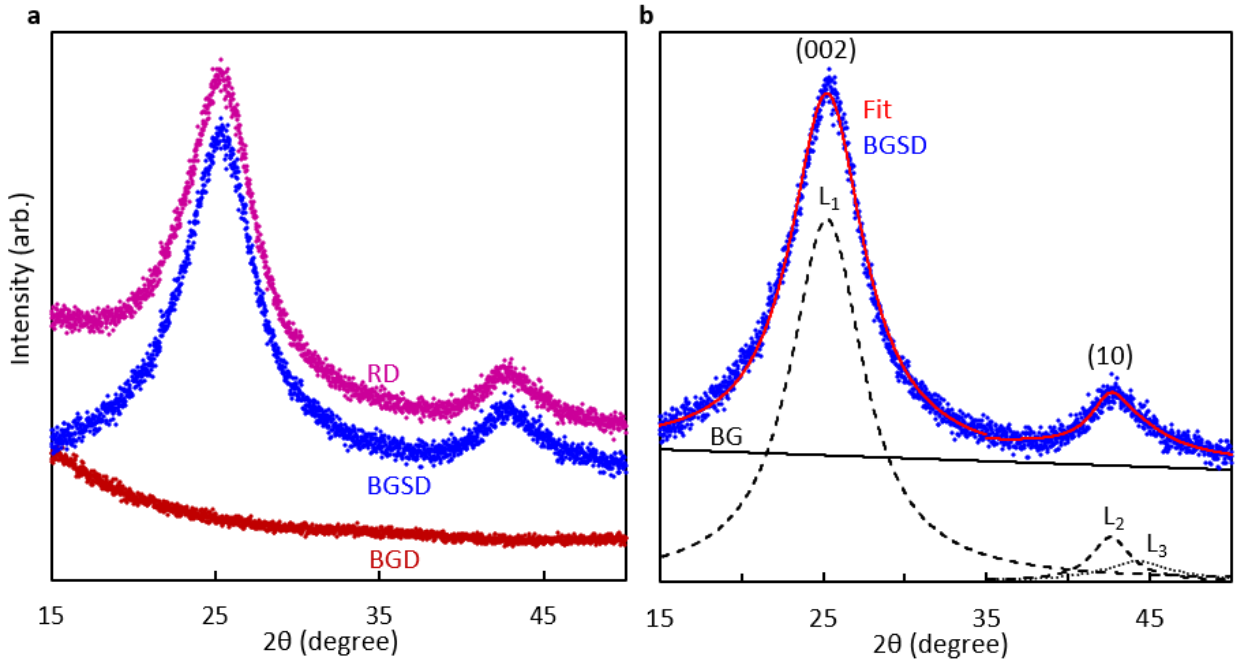

Figure S1. XRD pattern analysis. (a) The raw data (RD), measured background data (BGD), and background-subtracted data (BGSD) of BC_3' synthesized at 800 °C as a representative graphitic carbon material. (b) The BGSD fitted to the combination of a linear background (BG), a single Lorentzian (L_1) for the (002) reflection, and two Lorentzians for the (10) family of reflections (L_2 and L_3).

The peak center of L_1 was related to the d-spacing via Bragg's law, **Equation 1**, and the full-width at half-maxima (FWHM) of L_1 and L_2 were used to estimate the crystallite size in the c and a axes (referred to as L_c and L_a, respectively) via the Scherrer equation, **Equation 2**. The d-spacing and Scherrer size estimates based on the (002) reflection correspond to c-axis (layer-to-layer) ordering whereas the size estimate based on the (10) reflections corresponds to a-axis (in-plane) ordering.[S1]

$$d = \frac{1.54\ \text{Å}}{2 \sin \theta} \qquad (1)$$

$$L = \frac{0.9\,\lambda}{(\mathrm{FWHM})\cos\theta} \quad (2)$$

The FWHM in the Scherrer equation corresponds to the width of the reflection in 2θ, in radians. When plotting the resulting XRD patterns for comparison (**Figures 1a** and **2a** of the main text), the intensity of each pattern was normalized based on the maximum of the (002) reflection.

2. Raman Spectroscopy

The region containing the D and G peaks in each Raman spectrum was fitted using a previously established method based on the combination of a Lorentzian and a Breit-Wigner-Fano (BWF) line shape.[S2] The D peak was fitted to a single Lorentzian (referred to as L_4), the G peak was fitted to a single BWF, and the baseline was approximated by a linear background (BG), as shown in **Figure S2a**. The combination of a Lorentzian and a BWF provides a profile with minimal fitting parameters that can effectively fit the Raman spectrum of a wide range of graphitic carbon materials. The BWF line shape is given by **Equation 3**:

$$I(\omega) = \frac{I_o[1 + 2(\omega - \omega_o/Q\Gamma)]^2}{1 + [2(\omega - \omega_o/\Gamma)]^2} \quad (3)$$

where I_o is the peak intensity, ω_o is the peak position, Γ is the FWHM, and Q is the BWF coupling coefficient. A negative Q value tails the BWF toward lower frequency and accounts for residual intensity between the D and G peaks. Due to the asymmetry of the BWF line shape, ω_o does not lie at the frequency of the peak maximum (ω_{max}) as in a simple Lorentzian or Gaussian function. To correct for this, **Equation 4** was applied to determine ω_{max}. Since Q is negative, ω_{max} lies at a lower wavenumber than ω_o.

$$\omega_{max} = \omega_o + \frac{\Gamma}{2Q} \quad (4)$$

I(D)/I(G) was determined for each material based on the ratio of the peak maximum (I_o) of L_4 to that of the BWF. FWHM(D) and FWHM(G) were determined based on Γ of the L_4 and BWF fits, respectively. Pos(D) was determined based on ω_o of L_4 and Pos(G) was determined by applying **Equation 4** to ω_o of the BWF fit. The process for determining Disp(D) from a set of Raman spectra of varying E_L is demonstrated in **Figures S2b-d.** In this work, Raman spectra were collected at E_L = 532, 633, and 785 nm. The shift in Pos(D) as E_L decreases in energy is shown. The change in Pos(D) as a function of E_L is approximately linear, and the slope of this line is Disp(D) in units of cm^{-1} eV^{-1}.

When plotting the Raman spectra for comparison (**Figures S2c-d** as well as **Figures 1b** and **2b** of the main text), the intensity was normalized based on the maximum of the G peak.

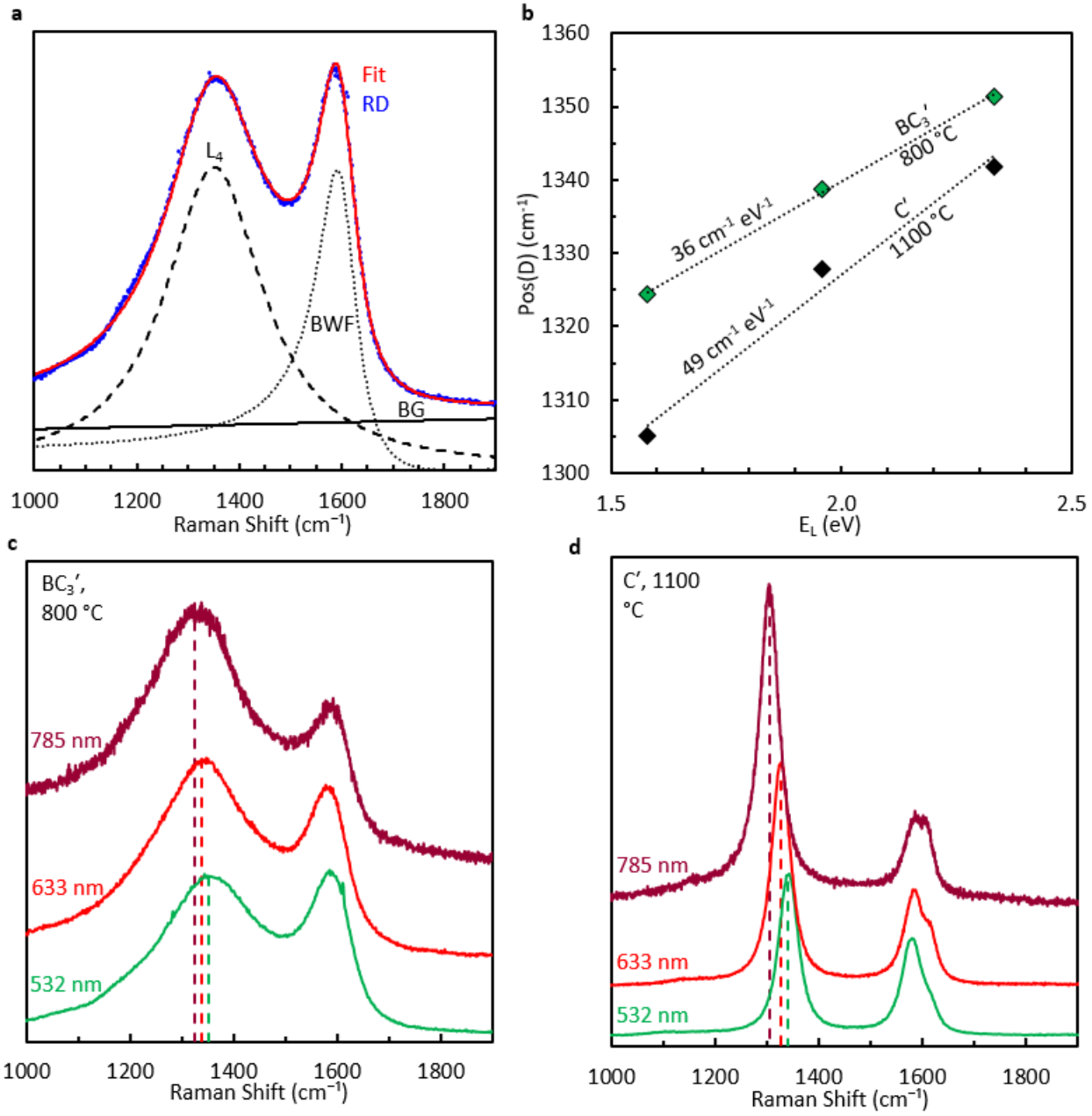

Figure S2. Raman spectrum analysis. (a) The raw data (RD) fitted to the combination of a linear background (BG), a single Lorentzian (L_4) for the D peak, and a single BWF for the G peak. The Raman spectrum of BC_3' synthesized at 800 °C (analyzed at $E_L = 532$ nm) is shown as a representative example. (b) The E_L dependence of Pos(D) used to calculate Disp(D) for two materials: (c) BC_3' synthesized at 800 °C and (d) C′ synthesized at 1100 °C.

3. X-Ray Absorption Spectroscopy (XAS)

Analysis of the XAS spectra was accomplished by dividing the measured total fluorescence yield (TFY) by the intensity of the incident X-ray beam. This accounts for fluctuations in beam intensity. The corrected spectrum was then normalized based on the pre- and post-edge step height. This provides a physically meaningful comparison between spectra since the pre-edge intensity corresponds to the minimum fluorescence observed and the post-edge intensity results from the excitation of a continuum of states within the bulk material and is expected to be relatively constant. The observed intensities of XAS features should not be directly related to concentrations of specific species within the sample since the scattering cross-sections for different excitations must be considered. As a result, the boron oxide signal observed in all materials investigated is disproportionately large.

The carbon K-edge of the BC_3' temperature series was also investigated to confirm the graphitic nature of the materials and is shown in **Figure S3**. The development of a strong angle-dependent π* absorption at 285.5 eV as well as a pronounced σ* transition at 292 eV shows evidence for ordering of the graphitic structure as synthesis temperature increases.

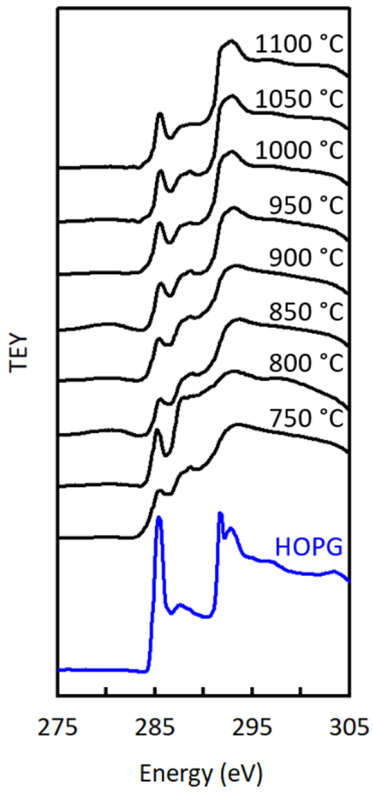

Figure S3: XAS carbon K-edge. Total electron yield (TEY) near the C K-edge of the BC_3' temperature series (black) compared to HOPG (blue) as a reference.

4. Energy Dispersive X-Ray Spectroscopy (EDX)

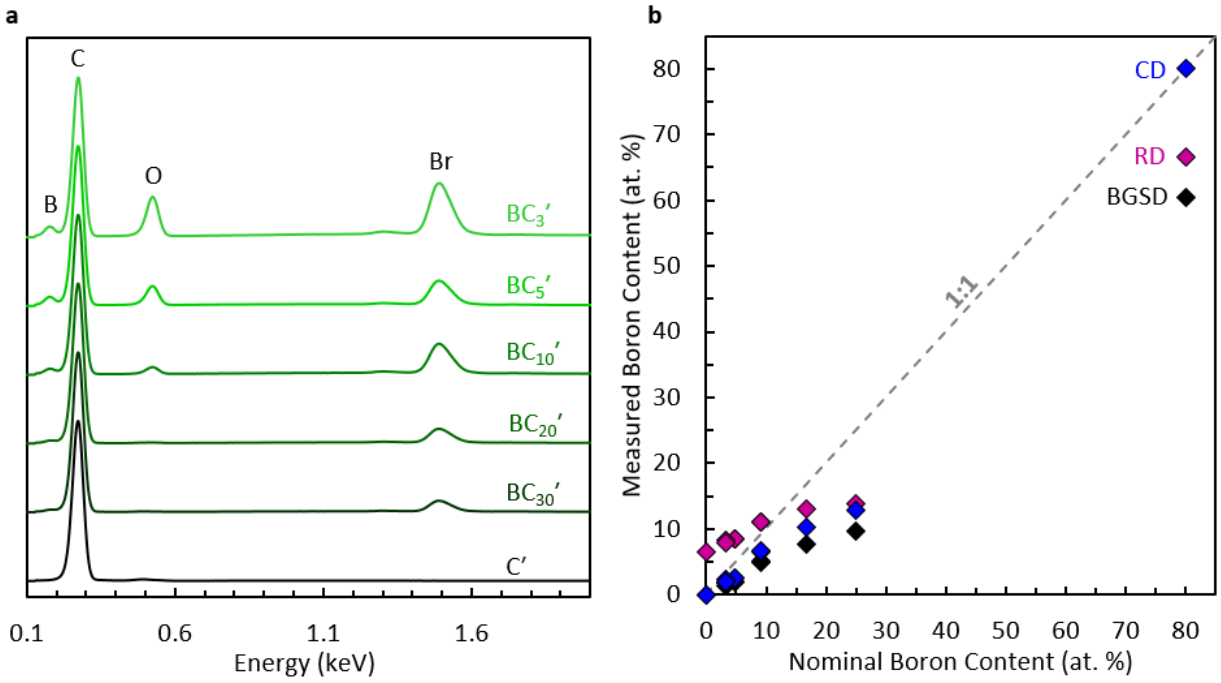

Figure S4. EDX spectrum analysis. (a) EDX spectra of the BC_x' composition series. (b) The boron content was determined for the BC_x' composition series as well as a boron carbide standard.

The raw EDX spectra of the BC_x' composition series are shown in **Figure S4a**. The intensities of the B Kα transition as well as the O Kα and Br Lα transitions increase as a function of nominal boron content. The boron content was determined using sensitivity factors for B, C, O, and Br as implemented by Bruker ESPRIT microanalysis software. As seen in **Figure S4b**, the raw data (RD) overestimate the amount of boron in the material at low compositions; as a result, it is necessary to apply a baseline subtraction (BGSD) to the measured boron content. A correction factor is then applied to the BGSD to bring the measured boron content of the boron carbide (B_4C) standard up to 80%. The corrected data (CD) show an incorporation limit of boron in carbon at ~11 at. %. The maximum amount of bromine measured in any BC_x' material was < 0.5 at. %.

5. Auger Electron Spectroscopy (AES)

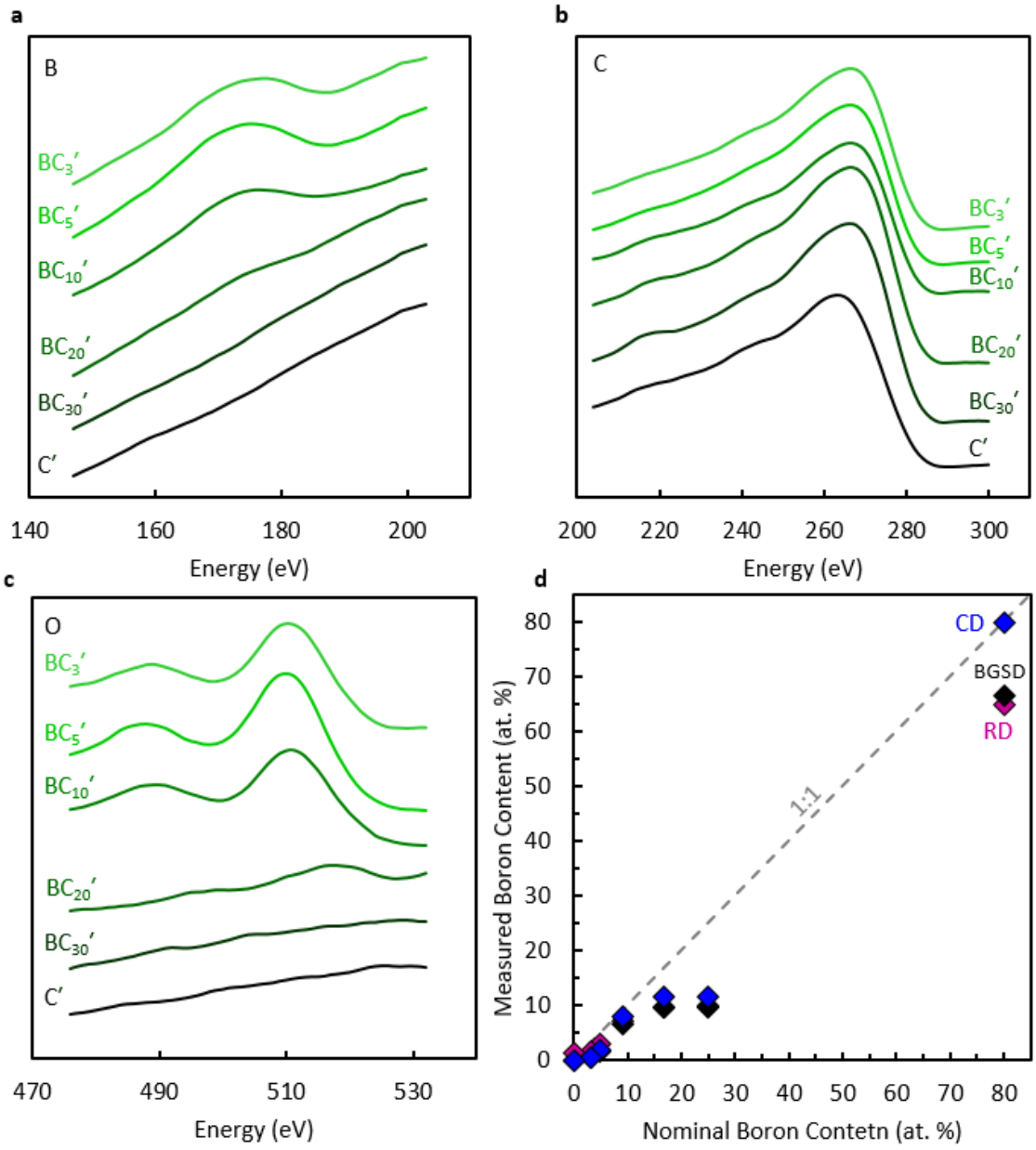

Figure S5. AES spectrum analysis. Raw AES spectra for the (a) B K-LL, (b) C K-LL, and (c) O K-LL transitions of the BC_x' composition series. (b) The boron content was determined for the BC_x' composition series as well as a boron carbide standard.

Auger electron spectra (AES) of the BC_x' composition series are shown in **Figures S5a-c**. In qualitative agreeance with EDX results, the intensity of the B KLL and O KLL transitions increase with increasing nominal boron content. Quantification of the smoothed and differentiated AES spectra was performed using sensitivity factors as implemented by PHI MultiPak analysis software. The raw data (RD) and background subtracted data (BGSD) are

shown in **Figure S5d**. A correction factor was applied to bring the measured boron content of a boron carbide standard (B_4C) up to 80%, shown as corrected data (CD).

6. Scanning Electron Microscopy (SEM)

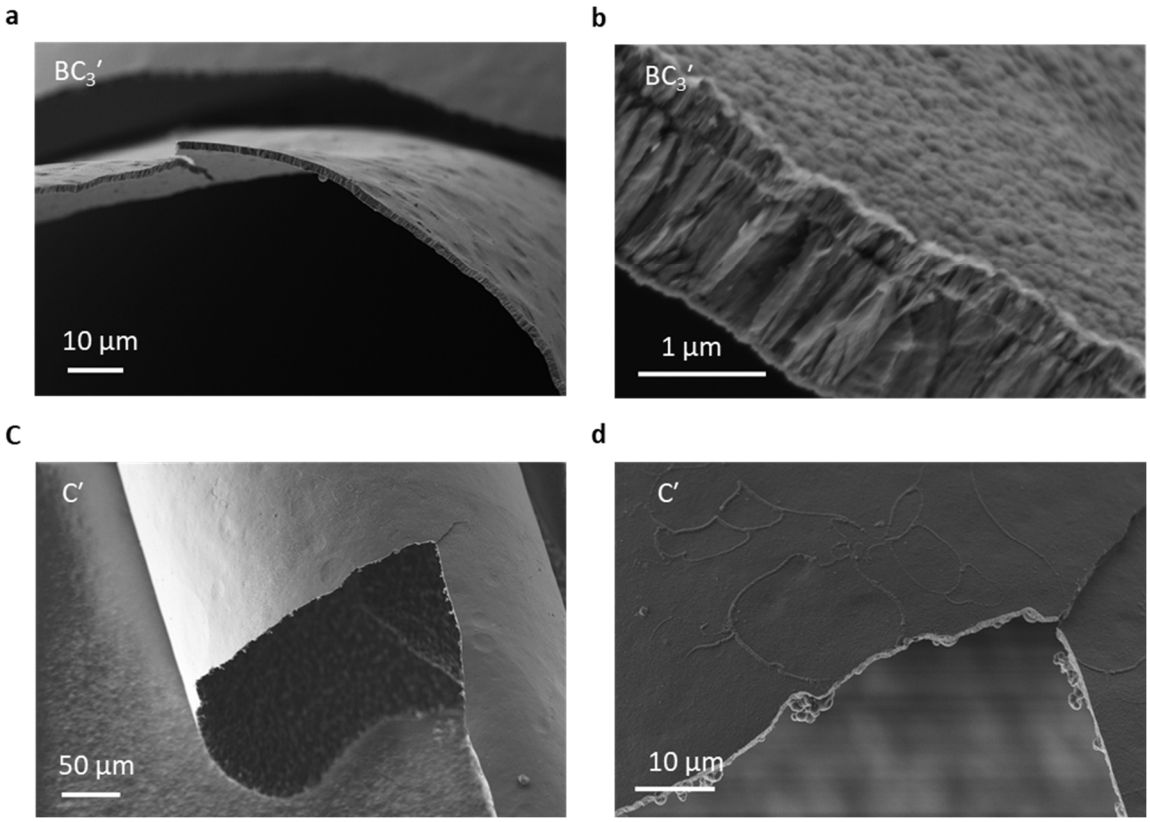

Figure S6. Scanning electron microscopy. SEM images of BC_3' (a) and (b), as well as SEM images of C' material (c) and (d).

Representative SEM micrographs of BC_3' and C' synthesized at 800 °C are shown in **Figure S6**. Two morphologies are observed in both the C' and BC_3' materials: flakes up to 1 cm in length and 1-2 µm thick, as well as carbonations spheres ~2 µm in diameter (seen on the underside of the C' flake in **Figure S6d**).

7. Phonon Dispersion Calculations

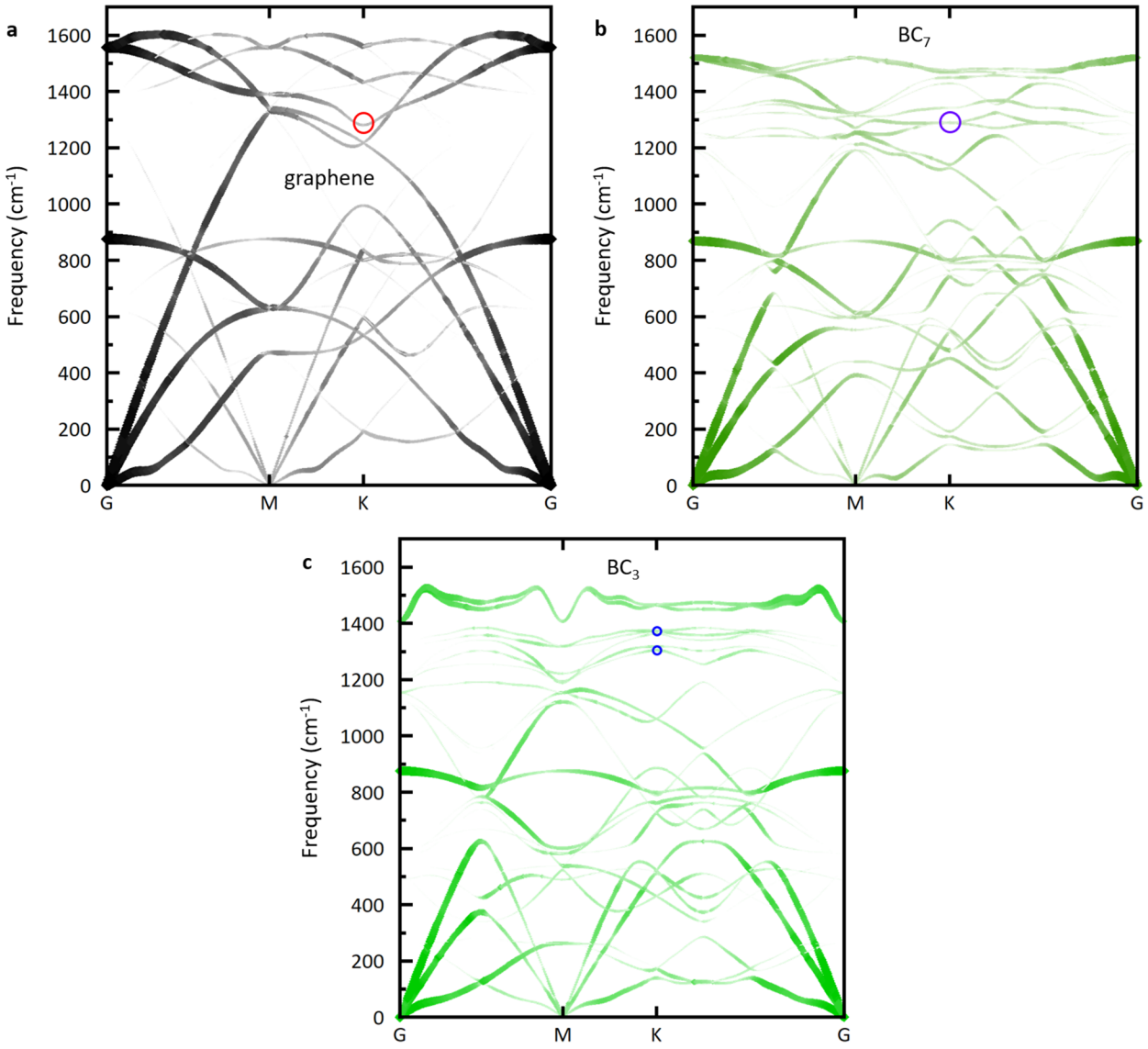

Figure S7. Calculated phonon dispersion diagrams for (a) graphene, (b) single-layer BC_7, and (c) single-layer BC_3. The optical modes (possibly) contributing to the D peak in the Raman spectrum of BC_x' are shown in the red, purple, and blue circles, respectively.

The unfolded phonon dispersion diagrams along the high-symmetry directions of the Brillouin zone for graphene, BC_7, and BC_3, calculated at the PBE level of DFT, are shown in **Figure S7**. The lattice motion associated with the high frequency TO phonon at the K point is illustrated for four phonons of interest likely to contribute to the D peak in the Raman spectrum of BC_x' in **Figure S8**. The TO phonon in graphene (red circle, **Figure S7a**), referred to as a "ring breathing" mode, exhibits A_{1g} symmetry (**Figure S8a**). The frequency of this phonon is calculated to be 1281 cm^{-1} at the K point, but exhibits a distinct Kohn anomaly

and therefore gives rise to a D peak with a strong dispersion relation. We note that the phonon dispersion diagram for graphene was calculated based on a supercell containing 8 atoms, and hence exhibits a number of spurious branches even after unfolding (including some apparent higher optical modes at the K point that are not physically meaningful).

A similar “ring breathing” mode is not present in single-layer BC_7 owing to reduced symmetry; there are no six-membered carbon rings exhibiting bonding environments with hexagonal symmetry. The six-fold axis of symmetry has been replaced by a three-fold axis. The highest symmetry vibrational mode at the K-point in this range of frequency shows breathing-like "ring distortion:" the three carbon-carbon bonds around the three-fold rotational axes elongate, while the three carbon-boron bonds remain stationary (**Figure S8b**). This mode exhibits a frequency of 1289 cm^{-1} at the K point (purple circle, **Figure S7b**). Both types of modes appear for single-layer BC_3 owing to the reemergence of six-fold axes of symmetry at the center of each pure carbon ring (blue circles, **Figure S7c**): a "ring breathing" mode at 1363 cm^{-1} (**Figure S8c**) and a "ring distorting" mode at 1304 cm^{-1} (**Figure S8d**). By symmetry considerations, only the "ring breathing" modes in graphene and BC_3 are truly comparable in their contributions to the position, intensity, and dispersion of the D peak measured in the Raman spectrum of graphitic BC_x' materials. The “ring breathing” mode at 1363 cm^{-1} in BC_3 is flat at near the K point and hence would give rise to a D peak with a negligible dispersion relation.

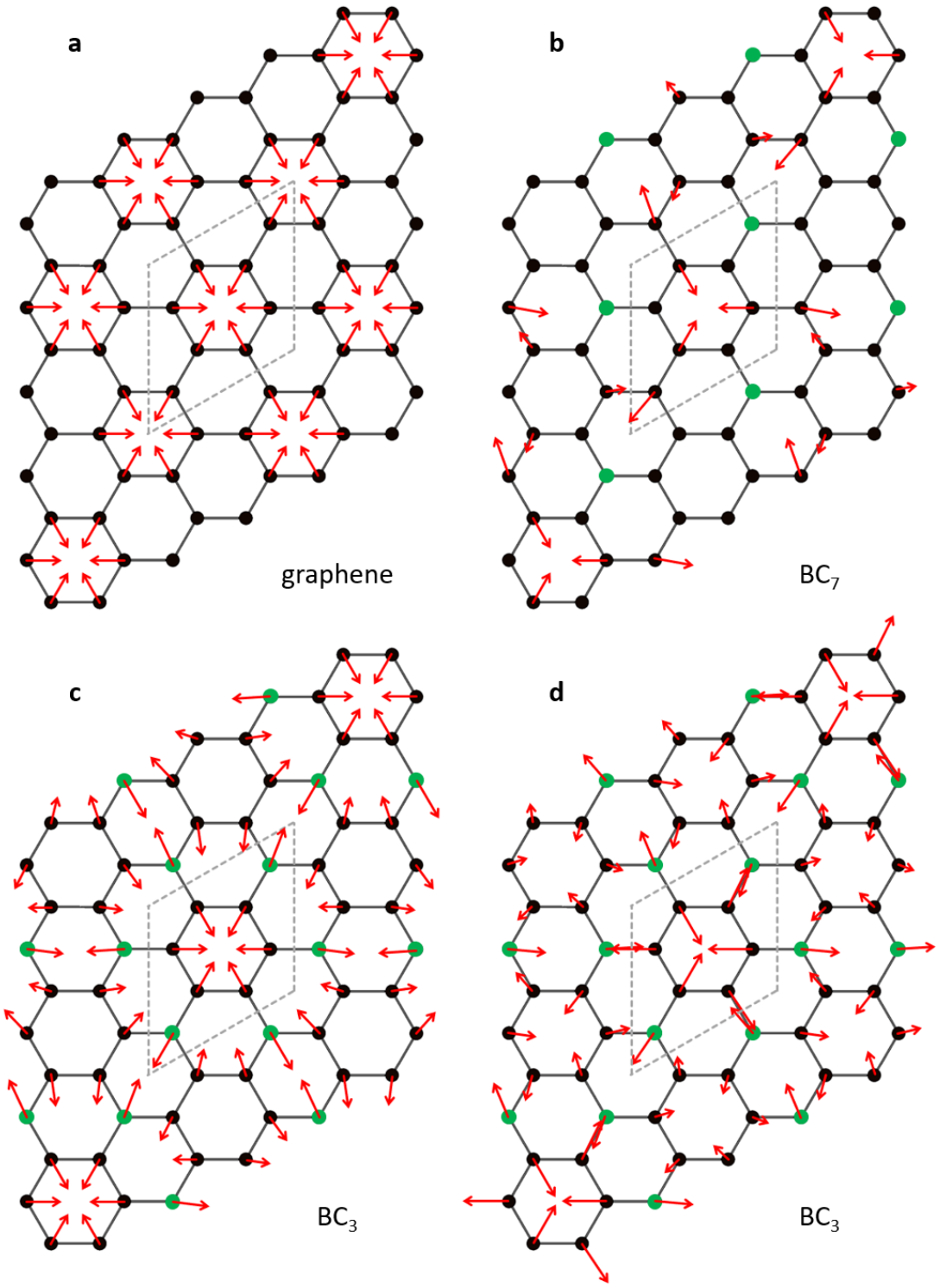

Figure S8. Vibrational modes corresponding to phonon branches of (a) graphene, (b) single-layer BC_7, and (c-d) single-layer BC_3 at near the measured D peak frequency in graphitic BC_x' materials, at frequencies of 1281, 1289, 1363, and 1304 cm^{-1}, respectively. Carbon is shown in black, boron in green, and the 8-atom cell used for calculations in gray.

8. Supporting References

S1. Langford, J. I. and Wilson, A. J. C. "Scherrer After Sixty Years: a Survey and Some New Results in the Determination of Crystallite Size." *J. Appl. Crystallogr.* **1978**, 11, 102-113.

S2. Ferrari, A. C. and Robertson, J. "Interpretation of Raman Spectra of Disordered and Amorphous Carbon." *Phys. Rev. B* **2000**, 61, 14095-14107.